13th ewtec 2019
Proceedings of the 13th European Wave and Tidal Energy Conference 1-6 Sept 2019, Naples, Italy

Model scale testing of multi-rotor arrays designed to exploit constructive interference effects

James McNaughton, Bowen Cao, Christopher R. Vogel, and Richard H.J. Willden

***Abstract*—Performance advantages from blockage are not currently accounted for in tidal turbine rotor and array design. Experiments have been performed to study the impact on performance of two identical rotors designed for, and operating in, high local blockage, when deployed in a large cross-section (low global blockage) tank. Tests were carried out on a single, and then two side-by-side, rotors in order to study the influence that local blockage has on the constructive interference between the rotors. This paper presents the impact that the second rotor has on the mean power and thrust coefficients. It is shown that at the design point, the power coefficient increases by 20% for a less than 10% increase in thrust. By operating the two turbines at different speeds it is shown that a further increase in power (up to 12%) can be achieved for one turbine by operating the neighbouring rotor at 1.5 times the thrust, which itself results in a reduction in power of the higher thrust turbine. At the design point flow is shown to accelerate significantly between and downstream of the two rotors, with similar though less extreme observations in the bypass regions. The results for performance and flow patterns follow trends that are observed in the literature for both theoretical and numerical studies, paving the way for industry to benefit from constructive interference in next generation turbine design.**

***Index Terms*—Tidal Turbines, Blockage, Constructive Interference, Experiments, Arrays**

I. Introduction

THE tidal energy sector has recently seen the installation of the first turbine arrays with Nova Innovation and MeyGen both successfully installing arrays of two (capacity 200 kW) and four (capacity 6 MW) turbines respectively. Multi-rotor floating systems have also gained momentum as they take advantage of shared support structures, grid connection, and some aspects of the power train. For example, Orbital Marine Power's 2MW SR2000 device has two rotors with shared power electronics on one platform, and Sustainable Marine Energy's PLAT-I uses four Schottel SIT250 turbines.

Placing rotors in close side-by-side configurations, coupled with the near proximity of the seabed and free surface, can lead to increased turbine performance. Garrett & Cummins [1] showed that the maximum power of an idealised turbine normalised by the undisturbed kinetic energy flux increased with the blockage ratio B (the ratio of the turbine swept area to cross-sectional area of the surrounding flow passage) as $\frac{16}{27}(1-B)^{-2}$, with the lower limit being the well-known Betz limit for the maximum performance of wind turbines. Nishino & Willden [2] considered the dynamics of turbine fences that partially extend across much wider channels, showing an up to 35% increase in an ideal turbine's performance if they are designed to take advantage of mutual blocking or so-called constructive interference effect. That a turbine's performance can increase in a blocked flow is not significant in itself. However, Schluntz & Willden [3] demonstrated that by incorporating blockage in the design process the benefits can be exploited further. More recently, Vogel & Willden [4] simulated a fence of four tidal turbines with a tip-to-tip spacing of 1D (diameter), demonstrating the variability of thrust and power across the fence due to different rotor designs and control strategies.

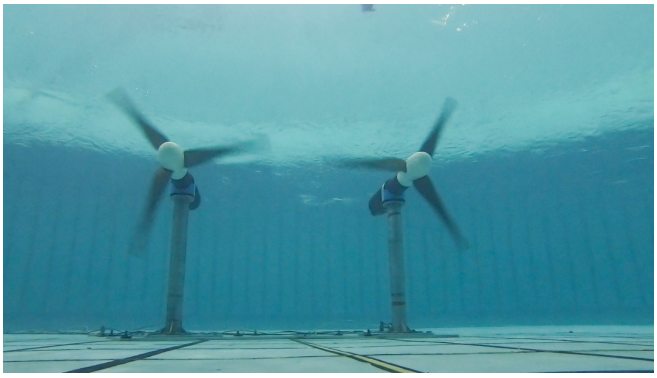

Fig. 1. Underwater photo of the two turbines operating side-by-side during the tests.

A multi-rotor fence system is currently being developed at the University of Oxford with the turbines designed to exploit the constructive interference effects. As part of the initial validation two identical rotors were constructed and tested in single and twin configurations at FloWave in the University of Edinburgh (see Fig. 1). This paper describes the experimental tests and presents results demonstrating the increased performance and loads arising from constructive interference.

II. Constructive interference

It is well understood that tidal turbines are sensitive to operating in blocked channels due to constraints on wake expansion [5], [6]. Constraining flow expansion results in accelerated flow in the bypass region that surrounds the core streamtube, which leads to a static

Paper ID 1338 submitted to Tidal device development and testing.
This work was supported in part by SuperGen and Wave Energy Scotland through Flex Fund projects 24865948 & 24866097 and an EPSRC grant no. EP/R007322/1.
The authors are all part of the Tidal Energy Research Group at the University of Oxford, Parks Road, Oxford, Ox1 3PJ, U.K. (corresponding author e-mail: james.mcnaughton@eng.ox.ac.uk).

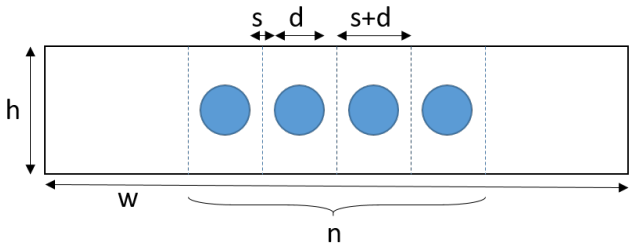

Fig. 2. Diagram showing dimensions used to define local and global blockage for n turbines in a fence (not to scale).

pressure gradient developing from upstream to downstream of the turbine. This streamwise static pressure gradient allows higher thrust levels to be achieved for the same through-turbine flow speed as the blockage ratio increases, or alternatively higher through-turbine speed for a given level of thrust. Generally, placing a turbine in an increasingly blocked flow will lead to higher performance until the flow becomes choked, i.e. the limiting point when an incremental increase in thrust no longer results in increased turbine power. However, through designing for the specific conditions a turbine is able to obtain even higher performance [3].

In the field it is proposed that tidal turbines will be able to achieve higher blockage ratio conditions through closely packing rotors together in a fence running perpendicular to the flow. Along with the seabed and free surface, turbines experience a constructive interference effect from the local blockage which is defined with the aid of Fig. 2 as:

$$B_L = \frac{A}{(s+d)h} \tag{1}$$

with D the turbine diameter, $A = \pi D^2/4$ the rotor area, s the tip-to-tip spacing between rotors and h the water depth. Similarly, the global blockage is defined as:

$$B_G = \frac{nA}{wh} \tag{2}$$

for n turbines in a channel of width w. Nishino & Willden [2] showed that for a fixed global blockage the performance can be altered significantly by varying the local blockage; indicating that performance enhancements from constructive interference is possible even for arrays of modest turbine numbers with very low levels of global blockage ratio. Maintaining a realistic and therefore low level of global blockage is important as channel geometry, depth variation, and the need for other channel uses, will prevent all but the lowest levels of global blockage for practical applications.

III. Turbine Model

A. Blade design

Tidal turbine blades are currently designed using similar approaches to that of wind turbines for unblocked environments (see for instance Wind Energy Handbook [7]). However, following the conclusion that turbines can benefit from constructive interference through careful placements, a rotor was designed for performance in high blockage conditions. The design method was performed with a blade element actuator disk method, embedded in a Reynolds-Averaged Navier Stokes solver (RANS-BE), with fine tuning of the design performed using blade resolved CFD. A general description of the approach can be found in [8].

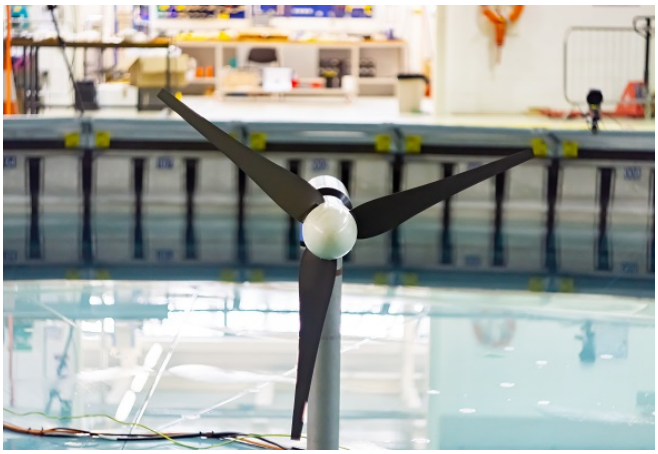

Fig. 3. Photo of assembled turbine model installed in the tank with the floor raised.

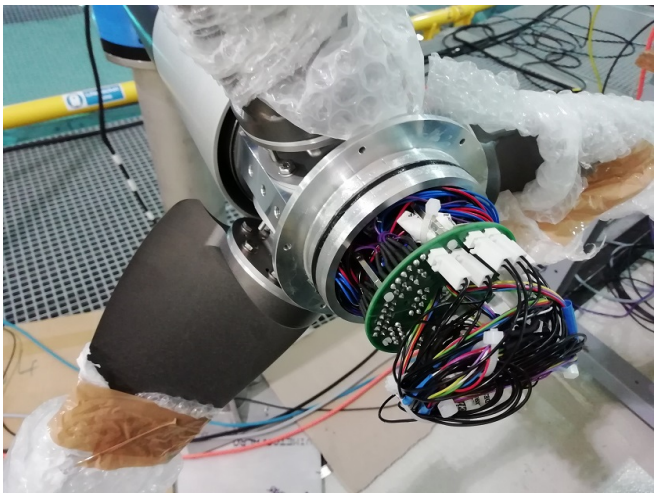

Fig. 4. Photo of nose section with nose cone and cover removed to reveal PCB for connecting strain gauges with amplifiers and connector to University of Edinburgh's nacelle.

The method leads to a design that has some obvious differences to the traditional turbine blade. Fig. 3 shows a close up frontal view of the rotor. One of the most noticeable differences between this design and the traditional blade is the large root section which helps maintain the desired blade loading distribution and control of spanwise variation of axial flow speed.

As the aim of the tests was to validate the design method and investigate the flow physics associated with constructive interference, the rotor did not require scaling as such, and was designed for this scale of tests specifically in order to select an aerofoil with suitable performance at relatively low Reynolds number (c. 200k based on blade chord at 70% span). A rotor diameter of 1.2 m was chosen to be reasonably large compared to the depth (2 m) which would ensure local blockage could be significant and help increase blade

Reynolds number, whilst not intending to affect the free surface.

Blades were manufactured on a CNC machine by an external company. Aluminium 6082-T651 was chosen as it can be machined easily, has a high maximum yield strength, and is pre-stressed which minimises the risk of deformation after being cut down. Despite this, the first test blade showed signs of bending under internal stresses once completed and for the remaining blades a large amount of material was cut away and then the piece left to rest before the final machining step. Although corrosion was not considered an issue for these tests, in order to preserve model life, and to protect from impact damage, the blades were hard anodised with a thickness of 30μ. The process both takes away material and adds thickness in roughly equal proportions, meaning that any variations to the blade design are much less than this value (and significantly lower than guideline tolerances [9], [10]).

B. Nacelle

The two rotors were connected to two of the University of Edinburgh's turbine nacelles, described in [11], [12]. These were originally designed for a 1.2 m diameter turbine with similar loads and so were very beneficial to de-risk the project as there was a great deal of knowledge and experience running and controlling these in the FloWave facility. The turbines are each controlled by a servo motor with a drive to control the speed through varying the torque; through this set up, the motor acts as a generator with the controller applying torque to slow control the shaft, similarly to the power take off for commercial wind and tidal turbines. Whilst expensive, this configuration means that more sophisticated control of the turbine is possible through use of the associated servo drives meaning speed and torque fluctuations can be minimised.

C. Instrumentation

The University of Edinburgh's nacelles were already equipped with a thrust and torque transducer and shaft encoder so rotor thrust, torque, speed, power and position were readily available. In addition, blade-root-bending-moment load cells were designed and manufactured, following a similar approach to those in [11], these were able to record the flapwise and edgewise loads on all three blades per turbine. Power and signals for the strain gauges were connected to a custom PCB (see 4), housed in the nose section, and combined onto a connector that could pass the signals directly though the nacelle and into the existing data acquisition software.

IV. Test set up

D. Test facility

The tests were performed in February 2019 at FloWave at the University of Edinburgh. The tank is circular with a diameter of 25 m and a depth of 2 m. A full description is given by Sutherland et al. [13], who characterised flow, profiles and turbulence at different locations and for different speeds. Other than for the Reynolds number dependency tests, a flow speed of 0.8 m/s was used as it was the value where the most detailed analysis was performed in [13], reducing the need for a study of the tank's flow field prior to the turbines being installed.

Due to the circular shape estimation of blockage is difficult for FloWave. The tank's diameter is known but for the region of straight flow the width varies meaning it is not useful to use the diameter as the width in (2). Moreover, the variable operation of the pumps around the perimeter causes recirculation zones, leading to a funnelling of the flow through the test region, which has an effective width less than the diameter but difficult to estimate, and likely to vary with turbine thrust. Assuming the width is 25 to 15 m, the global blockage is then estimated in the range of 4.5 to 7.5% for the twin turbine case. The local blockage is straightforward, and for the tip spacing of 0.25D, is 37%. The global blockage is higher in these tests than would be expected in a tidal farm ($< 1\%$ for a site several km across), although it is still deemed small enough such that the results will be predominantly dominated by the high local blockage as desired; as such no correction for global blockage has been made for the results.

E. Test matrix

The purpose of the tests was to investigate the influence that a second turbine, closely spaced to the side, has on a single rotor. To do so two turbines, hereafter referred to as the North and South turbines, were installed in two configurations, single and twin. For the single turbine test, only the North turbine was installed, and for the twin turbine test both North and South turbines were installed. The turbines were placed equally either side of the centreline with a tip spacing of 0.25D. For the single turbine configuration, the North turbine's position did not change, meaning the turbine was off-centre, although only slightly (0.75 m compared to the tank diameter of 25 m).

For both configurations, thrust and power performance curves were obtained by varying the speed of the rotors, known as a TSR (tip-speed ratio) sweep. As the exact upstream velocity was not known a priori during the tests, speed was controlled by defining the rpm, defined to give a suitable TSR range given the mean tank flow speed. For the twin configuration, performance curves were obtained by controlling both rotors at the same speed, as well as maintaining one at a fixed speed and varying the other.

Flow measurements were taken with an ADV, positioned at hub-height. For the performance tests the ADV was positioned 2D upstream of one rotor, for the twin case two TSR sweeps were performed with the ADV upstream of the North rotor in one case, and then upstream of the South rotor for the second case. In addition, a series of flow measurements, shown in Fig. 5, were taken with the turbines held at a constant speed, ω^*. For these tests a value of 77.5 rpm was

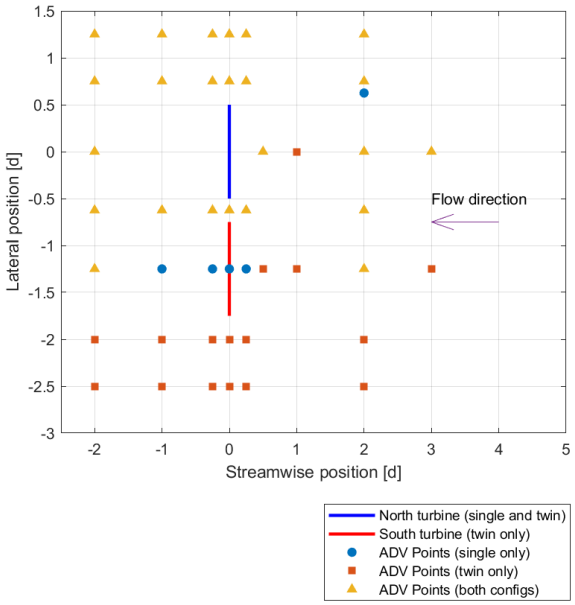

Fig. 5. Location of the ADV measurement points for the different test configurations.

chosen, giving an approximate TSR of 6.1 (see (4)) for $U = 0.8$ m/s, and hence:

$$\omega^* = \frac{\pi 77.5}{30}. \tag{3}$$

V. Analysis

F. Processing

In this paper results are restricted to average quantities for the entire rotor. In some cases, such as the discussion on flow speed, dimensional quantities are kept. For discussion on performance the TSR, power coefficient and thrust coefficients are used, defined respectively as:

$$\lambda = \frac{\omega R}{U} \tag{4}$$

$$C_P = \frac{P}{\frac{1}{2}\rho U^3 A} \tag{5}$$

$$C_T = \frac{T}{\frac{1}{2}\rho U^2 A} \tag{6}$$

where ω is the rotor speed, R the radius, P is the rotor power, T the rotor thrust and ρ is the fluid density taken at 1000 kg/m^3. Unless otherwise stated, U is measured $2D$ upstream of the rotor whose performance is being presented.

The turbine loads data was sampled at 256 Hz and the ADV flow data at 100 Hz, for the purpose of this analysis, the raw data is averaged over a 5-minute period. The correlation of the ADV signals was monitored and when it started to drop off seeding was added to the tank. It is also of note that the ADV showed a strong fluctuation in the lateral direction, likely induced by vortex induced vibrations on the support mechanism. The 5-minute average is sufficient to remove such noise in the flow data for these results,

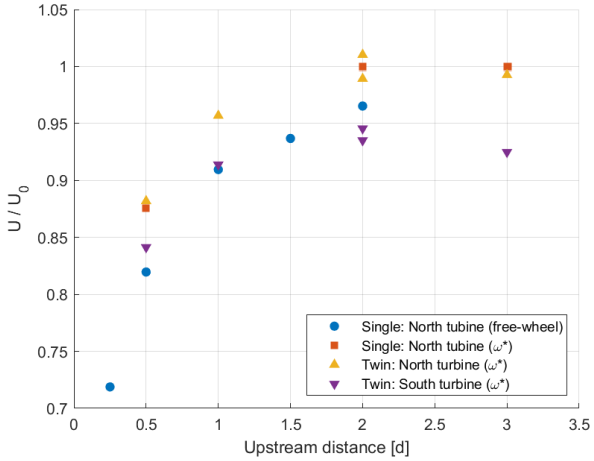

Fig. 6. Change in mean velocity along the centre-line upstream of the rotor for different tests and operating conditions.

although more detailed processing will be required for analysis considering shorter time periods and turbulent fluctuations. For the turbine thrust and torque data, a no-load offset is then subtracted before any further processing. The no-load value was recorded with the turbines in-situ on the tank floor, with no flow, each morning. In order to highlight the differences in results between single and twin turbine tests, where appropriate, values of C_P, C_T and U are normalised by their values for the single turbine operating at ω^*, respectively C_{P0}, C_{T0} and U_0 (which is measured $2D$ upstream of the rotor along the centreline).

G. Approach flow

Fig. 6 shows the mean normalised streamwise velocity upstream of the rotors for several test scenarios: North turbine in the single configuration for the free wheeling (low torque, high thrust) and ω^* speeds (high torque, low thrust), and the flow upstream of both North and South turbines in the twin configuration, controlled at ω^*. The flow has been normalised by U_0, which is the mean velocity $2D$ upstream of the single turbine operating at ω^*. Measurements are recorded at several upstream locations on the centreline of the subject rotor, although not all measurement points are taken for each case. As expected, the rotor causes flow to decelerate as it approaches the turbine, this is more pronounced for the free wheeling case where the rotor is exerting maximum thrust onto the flow. It is also observed that for single rotor there is an approximate 3.5% reduction in flow speed at 2D upstream for the higher thrust case.

The impact that the rotor has on the upstream flow is shown further in Fig. 7 which shows the streamwise flow at 2D upstream of the rotors as a function of the thrust coefficients for single and twin turbine configurations. There is an evident linear correlation between the upstream flow and the thrust coefficient, the impact of an adjacent rotor is accounted for by higher thrust which is discussed in more detail in later sections. It is also noted that there is around 4% variation in the single turbine's upstream flow speed for $\approx 50\%$ change

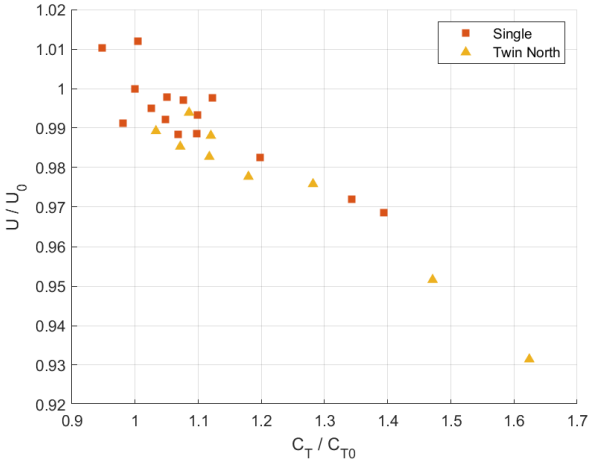

Fig. 7. Change in mean velocity 2D upstream of the rotor as a function of thrust coefficient.

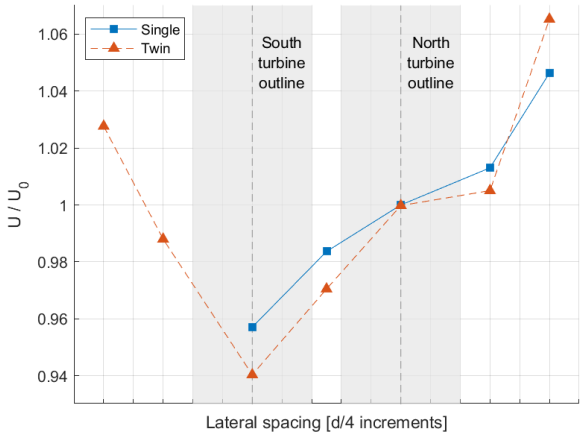

Fig. 8. Lateral variation in mean velocity 2D upstream of rotors (operating at ω^*).

in thrust. For the North turbine in twin configuration, the maximum variations in both quantities are almost double the maximums seen for the single turbine.

For the rotors operating at ω^*, Fig. 6 shows little variation in the flow from 2D to 3D upstream of the rotor, implying that this can be taken as the free-stream velocity for this case. Unfortunately the data point for the higher thrust case was not taken and so a conclusion cannot be made whether 2D upstream is suitable for defining the upstream flow for all cases.

It is also interesting to note that two data points were recorded with ADV 2D upstream of each turbine in the twin tests, and that the mean flow speed between these has changed, slightly, but significantly for analysis. Such variation can be caused by a variety of factors such as environmental conditions, slight changes in the tank control, or turbulent eddies in the flow. This highlights the importance of measuring the upstream flow concurrently with the turbine performance when both datasets are required for specific analysis (e.g. performance curves).

Fig. 6 also shows that the flow upstream of the North and South turbines is significantly different. To understand any lateral variation in the approach flow across the tank, transects were made at 2D upstream of the single and twin rotor configurations operating at a speed of ω^*. These transects are shown in Fig. 8, where each set of the duplicate points upstream of the twin rotors discussed above are averaged. For both cases it is clear that the flow is not laterally uniform and that there are differences in the flow once the second turbine was installed.

The flow upstream of the North turbine is close to the desired speed of 0.8 m/s for both the single and twin turbine cases. However, the flow upstream of the South turbine is lower. This has significant influence on the results as controlling both turbines to the same speed does not mean they are operating at the same TSR and hence will have different performance coefficients.

H. Reynolds number independence

As mentioned the rotor for these tests was designed for model scale, and so scaling the results is not an immediate priority. However, it is important to understand if the results can be applied to larger rotors for future work, and to understand if there are specific operating points in the tests where the blades are operating differently due to the Reynolds number. To do so a series of performance curves were obtained for the single rotor case at flow speeds of 0.6 to 0.9 m/s in 0.1 m/s increments. In all cases the ADV was fixed at 2D upstream of the rotor on the centreline. The flow of interest is that on the blade sections, rather than on the rotor itself, and so the chord-based Reynolds number at 70% of the blade span is used:

$$Re_{0.7} = \frac{c_{0.7} U \sqrt{1 + (0.7\lambda)^2}}{\nu} \tag{7}$$

with $c_{0.7}$ the chord length at 70% blade span and ν the kinematic viscosity (given a value of 1×10^{-6} m^2/s without loss of generality). To assess Reynolds number independence, the power coefficient is plotted against $Re_{0.7}$ in Fig. 9. Whilst there is some variation in the results, the peak performance and shape of the curves do not change with Reynolds number for these tests. It is also worth noting that, whilst $Re_{0.7}$ is used, the Reynolds number does not vary considerably up the blade due to the large taper offsetting the increase in relative velocity with an increase in radial position.

I. Rotor performance

This section presents results to compare the performance of the single rotor (North turbine), when the second (South turbine) is placed alongside it. Figs. 10 and 11 show the power and thrust coefficients for the North turbine as a function of TSR, respectively. Considering only the single configuration at first, the power curve is not entirely rounded with an obvious peak, as might be expected. This was partially due to some difficulties in maintaining control of the motor at lower speeds. The limiting speed was around 75 rpm,

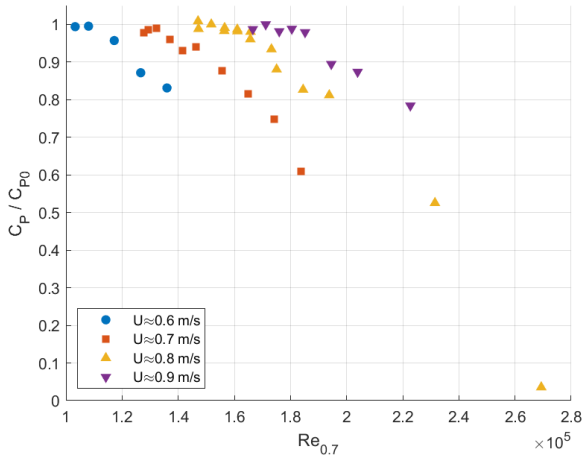

Fig. 9. Power coefficient as a function of Reynolds number at 70% span to demonstrate Reynolds independence of the model rotor and test conditions.

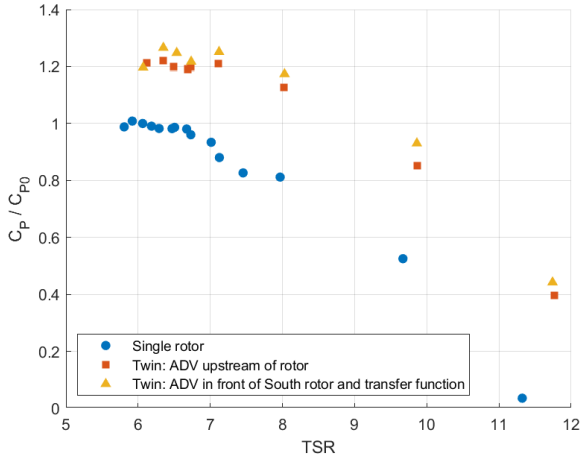

Fig. 10. Power coefficient as a function of tip-speed ratio for the North turbine in a variety of test conditions.

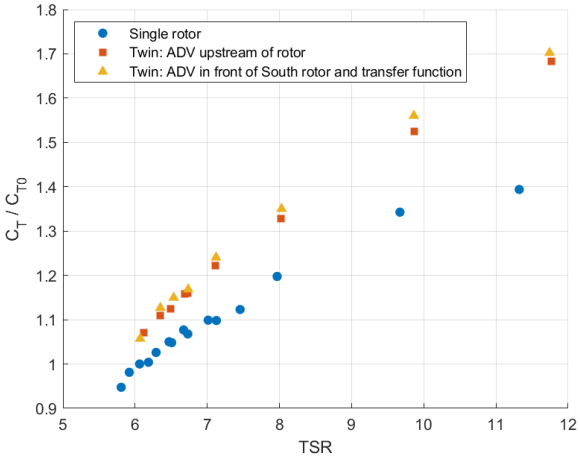

Fig. 11. Thrust coefficient as a function of tip-speed ratio for the North turbine in a variety of test conditions.

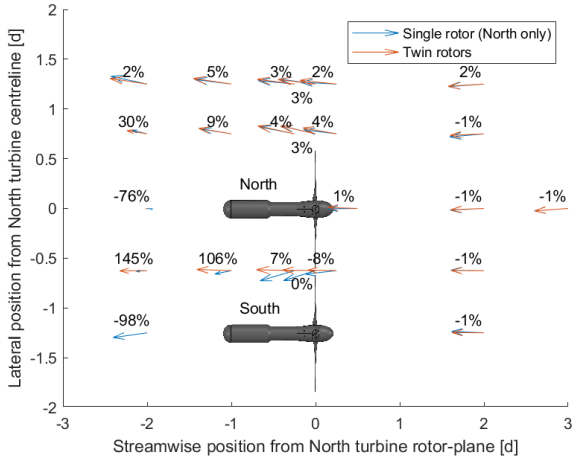

Fig. 12. Flow vectors around the North turbine for the single and twin turbine configurations. The numbers by each vector show the percentage change in flow speed from single to twin configurations.

although increased variance in the speed as this value was approached from above were clear. Nonetheless, it is clear that the presence of a second rotor leads to an increase in performance of around 20% at the maximum C_P point, with increases $< 10\%$ for thrust. The power curve is marginally shifted meaning that the optimal TSR increases slightly, as predicted by numerical simulations, as a greater rotational speed can be used to deliver a beneficial higher thrust in the twin turbine case. The C_P curve is also flatter for the twin configuration which indicates controlling at peak performance may be possible in fence configurations.

A second performance curve for the North turbine is shown for the twin configurations, which is created using the dataset when the ADV was upstream of the South rotor. As already discussed the flow is quite different upstream of the two rotors and so a transfer function was created using the ADV data for both TSR sweeps in the twin configuration. Using this approach it can be seen that a similar data set is obtained, although both power and thrust coefficients are overestimated.

Flow vectors around the North turbine are shown in Fig. 12 for both the single and twin configurations, and for clarity the percentage change in flow speed from single to twin configuration is also noted. The most noticeable changes occur between the rotors and in the downstream section just outside of the rotor plane. Between the rotors, where for the single case it is merely bypass flow, the flow in the twin rotor case is aligned to the streamwise direction and accelerates substantially downstream. In the bypass region on the other side of the turbine, the flow speed increases, more-so further downstream of the rotor disk. The flow speed reduction upstream, and increase in the bypass flow, that are observed for the twin turbine configuration match the trend as expected from theory and discussed earlier.

Controlling the rotors at fixed speeds, but with a velocity variation across the front of the array, means that in the twin configuration the rotors are operating at different TSRs and thus performance coefficients. To examine the impact of this, tests were performed maintaining the North turbine at a specific speed whilst varying the speed (and hence thrust) of the South

turbine. For the North turbine, two fixed speeds were examined. The first (ω^*) to maintain similarity with the rest of the test plan, and a second higher speed of $1.15\omega^*$ (chosen to give a TSR of 7 for $U = 0.8$ m/s) allowed for the South rotor to operate at both higher and lower control points to the North turbine. Figs. 13 and 14 show the variation of the North turbine's power and thrust coefficient against the South turbine's thrust coefficient respectively. The performance coefficients were all normalised according to their turbine-specific values for both turbines operating at the same speed of ω^*. For these tests the ADV was placed upstream of the North turbine and so a transfer function was used between velocities to calculate the South turbine's thrust coefficient. Referring to the difference between the twin configuration curves in Fig. 11 is thus useful in quantifying the uncertainty on the South turbine's thrust coefficients. There is a correlation between increasing the thrust on the South rotor, and an increase in both thrust and power on the North turbine. For the ω^* case, a 10% increase in thrust on the South rotor, the North rotor's power and thrust increase by approximately 6% and 5% respectively. After this initial step in varied performance, there is a control regime where increasing the South rotor's thrust does not provide as significant benefits to the North rotor, although it is also observed at this point the impact on North turbine's thrust is also minimal. For the higher speed case there are similar observations made regarding a linear increase in power and thrust of the North turbine against the South turbine's thrust. However, the step change that was seen for the ω^* speed is not present. At the extreme, as much as a 12% increase in power could be achieved by controlling the neighbouring turbine to a much higher (40-50%) level of thrust.

Whilst increasing the performance of the neighbouring turbine, increasing thrust will also have the negative effect of decreasing the performance of that turbine itself. Fig. 15 shows the averaged power coefficient of both turbines, i.e. the global power coefficient of the array, against the thrust of the South turbine. This has been calculated as the average of the normalised power coefficients:

$$C_{P-Ave} = \frac{1}{2}\left(\frac{C_{P-North}}{C_{P0-North}} + \frac{C_{P-South}}{C_{P0-South}}\right) \qquad (8)$$

with the normalisations $C_{P0-North}$ and $C_{P0-South}$ taken for both turbines operating at the same speed of ω^* as with Figs. 13 and 14. Whilst it is obvious that operating the turbines at very different control points away from the design conditions is detrimental for the averaged power, there appears to be an intermediate point where a thrust differential of 10% leads to an overall higher power coefficient for the array. It is not clear if this performance increase is linked to the non-uniform inflow meaning the turbine see a different flow, but it is an encouraging result and such observations are of interest when considering control strategies for multi-rotor fences.

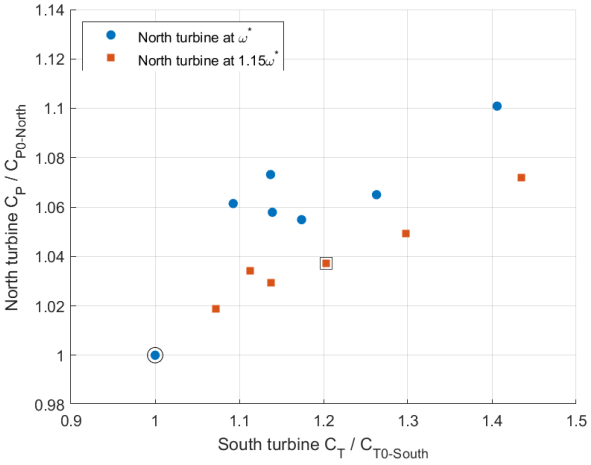

Fig. 13. Variation of North turbine's power coefficient as a function of the South turbine's thrust coefficient when North turbine is held at constant speed and South turbine varies speed. Outlined points indicate when both turbines are operating at the same speed.

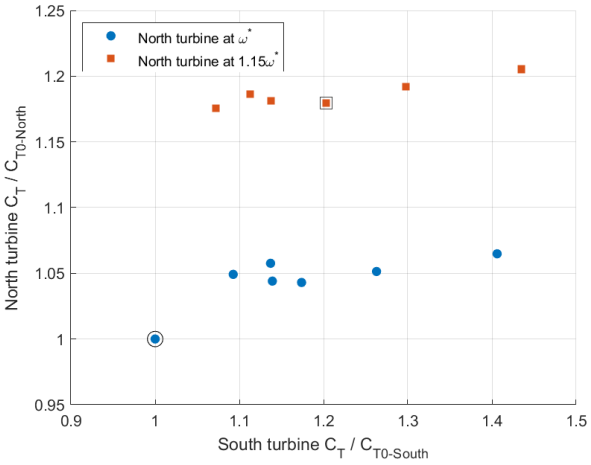

Fig. 14. Variation of North turbine's thrust coefficient as a function of the South turbine's thrust coefficient when North turbine is held at constant speed and South turbine varies speed. Outlined points indicate when both turbines are operating at the same speed.

VI. Discussion & Conclusions

This paper highlights the constructive interference effect on turbine performance arising from a high local blockage. Time-averaged results are presented to provide an initial assessment of the impact on thrust and power coefficients.

The power coefficient increases by approximately 20% around the design point due to the presence of an adjacent rotor, with a rise in thrust coefficient of less than 10%. Addition of the second rotor also indicates that the design TSR increases marginally. It is also shown that operating the twin rotors at different speeds can lead to significant performance variations, which will be relevant for overall multi-rotor fence system optimisation.

Analysis of the approach flow indicates that a measurement point 2D upstream of the rotors should be representative of the free stream flow, although this varies with turbine thrust so cannot be considered undisturbed, and indicated for performance tests it is

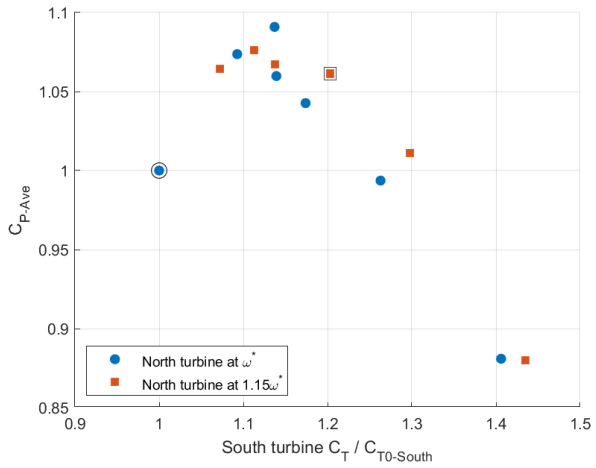

Fig. 15. Variation of averaged power coefficient for both North and South turbines as a function of the South turbine's thrust coefficient when North turbine is held at constant speed and South turbine varies speed. Outlined points indicate when both turbines are operating at the same speed.

necessary to record the upstream flow synchronously with turbine thrust at all control points. As test time was limited it was not possible to perform measurements with the ADV in as many upstream positions as was desired. The decision to position the ADV at 2D upstream of the rotors for the majority of tests came following best practice from other tests performed at FloWave (e.g. [14]) as well as the IEC 62600-200 guidelines [15]. Having shown the influence of the rotors on the flow at the upstream point, an area of future work will be to investigate this more extensively. For these tests it was also observed that the lateral flow 2D upstream of the rotor was not uniform which had the undesirable effect of both rotors not being at the same operating point (as defined by C_P and C_T), despite being controlled at the same rotational speed.

Qualitatively, trends predicted by theory have been demonstrated experimentally, both in terms of increased performance with local blockage and modification of flow field due to inter-turbine flow accelerations. The next steps will be to conduct a more thorough analysis of the data set, particularly analysing the root-bending moment data and performing a more detailed study on the influence of unsteadiness from blade position and flow variations. Numerical work in [8] indicates that the peak performance for the turbine is for a TSR between 5 and 6, although this could not be verified in these tests due to the difficulty in controlling the turbine at lower speeds corresponding to a TSR¡6. As the global blockage for FloWave was difficult to define, further numerical studies are currently being performed that will model the rotors at the correct local and global blockages, so that a thorough assessment of the numerical design approach can be performed and to understand where any differences arise from.

The next stage in the project's development will be better understand the influence of local blockage on the constructive interference effect through varying rotor spacing, and understand the impact of fence length, through testing rotors against walls or baffle plates to act as a symmetry plane. Future tests will hope to remove some of the uncertainty on the results due to the non-uniform upstream flow, and provide more stable control for lower rotational speed.

ACKNOWLEDGEMENT

The authors would like to thank Atlantis SIMEC Energy for useful comments and discussions; Gregory Payne, Tim Stallard and Jeff Steynor for guidance in rotor design; Tom Davey, Anup Nambiar and Edd Nixon for their support prior to and throughout the tests; the University of Edinburgh for loaning two of their nacelles for use in the project; Steven Ettema, Federico Zilic de Arcos and Daniela Taira for their contributions to the testing.

REFERENCES

[1] C. Garrett and P. Cummins, "The efficiency of a turbine in a tidal channel," *Journal of Fluid Mechanics*, vol. 588, pp. 243–251, 2007.
[2] T. Nishino and R. H. J. Willden, "Two-scale dynamics of flow past a partial cross-stream array of tidal turbines," *Journal of Fluid Mechanics*, vol. 730, pp. 220–244, 2013.
[3] J. Schluntz and R. H. J. Willden, "The effect of blockage on tidal turbine rotor design and performance," *Renewable Energy*, vol. 81, pp. 432–441, 2015. [Online]. Available: http://dx.doi.org/10.1016/j.renene.2015.02.050
[4] C. R. Vogel and R. H. Willden, "Multi-rotor tidal stream turbine fence performance and operation," *International Journal of Marine Energy*, vol. 19, pp. 198–206, 2017. [Online]. Available: https://doi.org/10.1016/j.ijome.2017.08.005
[5] A. S. Bahaj, A. F. Molland, J. R. Chaplin, and W. M. J. Batten, "Power and thrust measurements of marine current turbines under various hydrodynamic flow conditions in a cavitation tunnel and a towing tank," *Renewable Energy*, vol. 32, no. 3, pp. 407–426, 2007.
[6] B. Gaurier, G. Germain, J. V. Facq, C. M. Johnstone, A. D. Grant, A. H. Day, E. Nixon, F. D. Felice, and M. Costanzo, "Tidal energy Round Robin " tests comparisons between towing tank and circulating tank results q," *International Journal of Marine Energy*, vol. 12, pp. 87–109, 2015. [Online]. Available: http://dx.doi.org/10.1016/j.ijome.2015.05.005
[7] T. Burton, N. Jenkins, D. Sharpe, and E. Bossanyi, *Wind Energy Handbook*. Chichester, UK: John Wiley & Sons, Ltd, may 2011, ch. 3, pp. 68–93. [Online]. Available: http://doi.wiley.com/10.1002/9781119992714
[8] B. Cao, R. H. J. Willden, and C. R. Vogel, "Effects of blockage and freestream turbulence intensity on tidal rotor design and performance," in *3rd International Conference on Renewable Energies Offshore*, 2018.
[9] ITTC, "7.5-01-01-01 Model Manufacture Ship Models," 2002.
[10] ITTC, "7.5-02-07-03.9 Model Tests for Current Turbines," 2014.
[11] G. S. Payne, T. Stallard, and R. Martinez, "Design and manufacture of a bed supported tidal turbine model for blade and shaft load measurement in turbulent flow and waves," *Renewable Energy*, vol. 107, pp. 312–326, 2017.
[12] G. S. Payne, T. Stallard, R. Martinez, and T. Bruce, "Variation of loads on a three-bladed horizontal axis tidal turbine with frequency and blade position," *Journal of Fluids and Structures*, vol. 83, pp. 156–170, 2018. [Online]. Available: https://doi.org/10.1016/j.jfluidstructs.2018.08.010
[13] D. Sutherland, D. R. Noble, J. Steynor, T. Davey, and T. Bruce, "Characterisation of current and turbulence in the FloWave Ocean Energy Research Facility," *Ocean Engineering*, vol. 139, no. February, pp. 103–115, 2017.
[14] S. Draycott, G. Payne, J. Steynor, A. Nambiar, B. Sellar, and V. Venugopal, "An experimental investigation into non-linear wave loading on horizontal axis tidal turbines," *Journal of Fluids and Structures*, vol. 84, pp. 199–217, 2019. [Online]. Available: https://doi.org/10.1016/j.jfluidstructs.2018.11.004
[15] IEC TS 62600-200:2013, "Marine energy - Wave, tidal and other water current converters - Part 200: Electricity producing tidal energy converters - Power performance assessment," 2013.